Comparison of Chlorpyrifos-Oxon and Paraoxon Acetylcholinesterase Inhibition Dynamics: Potential Role of a Peripheral Binding Site

A. A. Kousba,* L. G. Sultatos,† T. S. Poet,* and C. Timchalk,*,[1]

*Battelle, Pacific Northwest Division, Richland, Washington 99352, and †University of Medicine and Dentistry New Jersey, Newark, New Jersey

The primary mechanism of action for organophosphorus (OP) insecticides, like chlorpyrifos and parathion, is to inhibit acetylcholinesterase (AChE) by their oxygenated metabolites (oxons), due to the phosphorylation of the serine hydroxyl group located in the active site of the molecule. The rate of phosphorylation is described by the bimolecular inhibitory rate constant (k_i), which has been used for quantification of OP inhibitory capacity. It has been proposed that a peripheral binding site exists on the AChE molecule, which, when occupied, reduces the capacity of additional oxon molecules to phosphorylate the active site. The aim of this study was to evaluate the interaction of chlorpyrifos oxon (CPO) and paraoxon (PO) with rat brain AChE to assess the dynamics of AChE inhibition and the potential role of a peripheral binding site. The k_i values for AChE inhibition determined at oxon concentrations of 1–100 nM were 0.206 ± 0.018 and 0.0216 nM^{-1}h^{-1} for CPO and PO, respectively. The spontaneous reactivation rates of the inhibited AChE for CPO and PO were 0.084–0.087 (two determinations) and 0.091 ± 0.023 h^{-1}, respectively. In contrast, the k_i values estimated at a low oxon concentration (1 pM) were ~1,000- and 10,000-fold higher than those determined at high CPO and PO concentrations, respectively. At low concentrations, the k_i estimates were approximately similar for both CPO and PO (150–180 [two determinations] and 300 ± 180 nM^{-1}h^{-1}, respectively). This implies that, at low concentrations, both oxons exhibited similar inhibitory potency in contrast to the marked difference exhibited at higher concentrations. These results support the potential importance of a secondary peripheral binding site associated with AChE kinetics, particularly at low, environmentally relevant concentrations.

Key Words: acetylcholinesterase; organophosphate insecticide; chloropyrifos oxon; paraoxon.
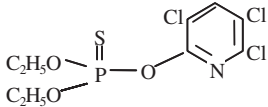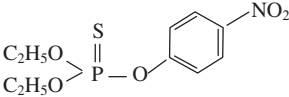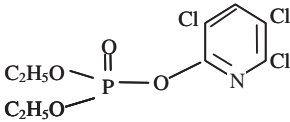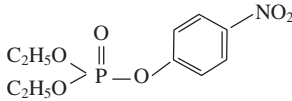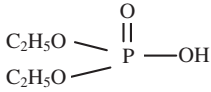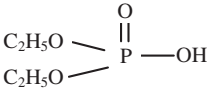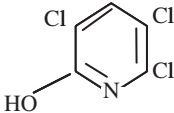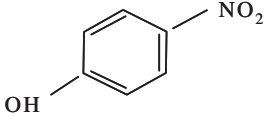
Chlorpyrifos and parathion are organophosphorus (OP) insecticides that have been used extensively in pest control. OP insecticides share common metabolic processes and toxicity mechanisms (Sultatos and Murphy, 1983), primarily involving irreversible inhibition of acetylcholinesterase (AChE) by active oxon metabolites (chloropyrifos-oxon [CPO] and paraoxon [PO]). This results in a range of neurotoxic effects due to the accumulation of acetylcholine within cholinergic synapses (Mileson *et al.*, 1998). The metabolic activation of these OP insecticides involves CYP450-mediated oxidative desulfuration to CPO and PO and detoxification by CYP450-mediated dearylation producing the major metabolites trichloropyridinol and *p*-nitrophenol, respectively (McCracken *et al.*, 1993; Poet *et al.*, 2003; Sultatos and Murphy, 1983). The chemical structure of these insecticides and their key metabolites are given in Table 1. The balance between desulfuration and dearylation can result in very different levels of AChE inhibition (Timchalk, 2001, 2002).

Both CPO and PO are electrophilic compounds that phosphorylate the serine hydroxyl group located in the active site of AChE. The phosphorylation yields a stable, inactive enzyme. The inhibitory bimolecular rate constant (k_i) describes the rate of cholinesterase (ChE) phosphorylation and the inhibitory potency of OPs (Amitai *et al.*, 1998; Carr and Chambers, 1996; Kardos and Sultatos, 2000; Kousba *et al.*, 2003; Rosenfeld *et al.*, 2001). *In vitro* k_i determinations have been based on the method developed by Main (1964) in which high oxon concentrations are incubated with ChE, assuming that the reaction approximates first-order conditions. Kardos and Sultatos (2000) have suggested that this approach was inadequate to describe the interaction of PO with AChE over a wide range of concentrations, and have suggested that a peripheral binding site might exist that, when occupied, reduces the capacity of additional oxon molecules to phosphorylate the active site. Therefore, the use of high oxon concentrations in this assay may result in an extremely rapid inhibition of ChE, which may be a potential important source of error in k_i determinations. An alternate approach to describe the dynamics of ChE inhibition uses a modified Ellman assay in conjunction with a pharmacodynamic model to determine the k_i (Kardos and Sultatos, 2000; Kousba *et al.*, 2003). The major advantage of this approach is the ability to determine the k_i using any OP concentration relative to the cholinesterase concentration where the reactions follow either first- or second-order kinetics, a condition that can not be satisfied using the previous approaches (Kardos and Sultatos, 2000).

[1] To whom correspondence should be addressed at Battelle, Pacific Northwest Division, 902 Battelle Boulevard, P.O. Box 999, Richland, WA 99352. Fax: (509) 376-9064. E-mail: charles.timchalk@pnl.gov.

TABLE 1
Comparison of Chemical Structure of Chlorpyrifos, Parathion, Critical Metabolic Products, and Acute Toxicity

Common name	Chlorpyrifos	Parathion
Chemical Name	O,O-diethyl-O-(3,5,6-trichloro-2-pyridyl) phosphorothioate CAS[#] 2921-88-2	O,O-diethyl-O-(2-isopropyl-4-methyl-6-pyrimidinyl)-phosphorothioate CAS[#] 333-41-5
Chemical Structure		
Active Metabolite (Oxon)		
Phosphorylating Group	Diethyl phosphate	Diethyl phosphate
Leaving Group (biologically inactive metabolite)	3,5,6-trichloro-2-pyridinol (TCP)	P-nitrophenol
Acute Toxicity (LD$_{50}$) (oral, male rat) mg/kg	$\sim$82–155	4–13

Concentration-dependent k_i values have been attributed to the possible existence of a secondary binding site (Kardos and Sultatos, 2000), which may or may not be related to the peripheral binding site identified on the surface of the AChE molecule. Early studies of the hydrolysis of acetylcholine by AChE documented substrate inhibition by acetylcholine and suggested an allosteric mechanism (Changeux, 1966). Taylor and Lappi (1975) first identified a peripheral binding site for AChE, which likely results in substrate inhibition when occupied. Subsequent studies have established the existence of this peripheral binding site on the surface of the enzyme, about 20 Å from the entrance to the active site (Berman *et al.*, 1980). This peripheral binding site has been considered as an obligatory landing site for charged ligands, a part of the active site, an ionic strength sensor (Berman and Leonard, 1992), and the site of excess substrate inhibition. Taylor and Radic (1994) have suggested that ligand association with the peripheral binding site may prevent access of substrates to the active site by physical obstruction, charge repulsion with the association of a cationic ligand, or by an allosteric mechanism in which the active center conformation is altered. While several ligands in addition to acetylcholine have been shown to bind to the peripheral binding site, most OPs have been thought not to occupy this site since they have been reported to follow simple second-order kinetics (Friboulet *et al.*, 1990). However, Kardos and Sultatos (2000) have suggested that PO and methyl PO likely bind to a site distinct from the active site and that occupation of the site makes subsequent phosphorylation of the active site more difficult. However, they did not determine if this putative secondary site is identical to or overlaps with the well-characterized peripheral binding site.

The aim of our study was to compare the dynamics of AChE inhibition following *in vitro* incubation with CPO or PO, over a wide range of concentrations, to help elucidate the presence of a peripheral binding site. The selection of CPO and PO was based on several factors including similarities in

chemical structures, mechanism of actions, and common metabolic pathways as well as chemically identical enzyme inhibition complexes (Table 1).

MATERIALS AND METHODS

Chemicals. Chloropyrifos oxon ([*O,O*-diethyl-*O*-(3,5,6-trichloro-2-pyridinyl) phosphate]) and paraoxon (*O,O*-diethyl-*O*-(*p*-nitrophenyl) phosphate) were purchased from Chemical Services, Inc. (West Chester, PA); 5,5,-dithio-bis 2-nitrobenzoic acid (DTNB) and acetylthiocholine (ATC) were purchased from Sigma Chemical Co. (St. Louis, MO). The remaining chemicals used in this study were reagent grade or better and were also purchased from Sigma Chemical Co.

Animals. Male Sprague-Dawley rats that were 3 months old (weighing 300–350 g) were purchased from Charles River Lab Inc. (Raleigh, NC). Prior to use, animals were housed in solid-bottom cages with hardwood chips (Laboratory grade SANI chips, TEKLAD, Madison, WI) under standard laboratory conditions and given free access to water and food (PMI 5002, Certified Rodent Diet, Animal Specialities, Inc., Hubbard, OR). All procedures involving animals were in accordance with protocols established in the NIH/NRC *Guide and Use of Laboratory Animals* and were reviewed by the Institutional Animal Care and Use Committee at Battelle, Pacific Northwest Division.

Tissue preparations. Rats were weighed, humanely sacrificed by CO_2 asphyxiation, and individual rat brains were immediately removed, rinsed in ice-cold buffer, weighed, and homogenized in 9 volumes of 0.1 M phosphate buffer (pH 7.4) using a polytron homogenizer (Brinkman Instruments, Westbury, NY). The brain homogenates were stored as individual 1-ml aliquots at −80°C until the time of ChE activity determination. Preliminary studies detected no differences in AChE activity in both fresh and frozen homogenates, provided homogenates were not kept frozen longer than 3 months (data not shown).

Characterization of brain AChE activity profile and enzyme kinetics. The brain homogenates were thawed at room temperature and an aliquot was diluted in an additional 6 volumes of phosphate buffer. Next, 200 μl diluted homogenate were incubated with 200 μl phosphate buffer containing a range of CPO (1×10^{-3}–25 nM) or PO (5×10^{-4}–100 nM) concentrations in a shaker at room temperature for 0–24 h. The dilution of brain homogenate was used to place the absorbance between 0.1 and 1 OD/min. Reactions were terminated by the addition of 4.6 ml phosphate buffer to each brain sample. Brain AChE activity was determined by a modified Ellman method (Ellman *et al.*, 1961) using a 96-well automated microplate spectrophotometer ELx808 equipped with a KC4 software package (Bio-Tek Instruments, Inc., Winooski, VT). Sample (250 μl/well) was transferred and 25 μl of DTNB and ATC were placed in each well for final concentrations of 0.1 and 0.4 mM of DTNB and ATC, respectively, and a final volume of 300 μl/well (Mortensen *et al.*, 1996; Nostrandt *et al.*, 1993). The control samples were incubated with phosphate buffer that did not include any oxon. The AChE activity described by the rate of ATC hydrolysis was monitored by following the absorbance profile at 405 nm over 30–40 min. The slope of the linear regression of that profile was used to measure the remaining enzyme activity. The statistical analysis of the data was limited to a determination of a mean and standard deviation of three samples where appropriate by using the standard equations.

The 50% inhibitory concentration values (IC_{50}) for CPO and PO were determined under identical experimental conditions with respect to homogenate dilution, homogenate/buffer incubation ratio and time, and substrate concentrations. Diluted brain homogenate (200 μl) was incubated with equal amounts of buffer containing a range of oxon concentrations in a shaker at room temperature for 5 min; the reactions were terminated and AChE activity was determined as described above. Control samples incubated with buffer but containing no oxon were also included. The IC_{50} values were calculated using the pharmacokinetic software WinNonlin version 1.1 (Pharsite Corp., Cary, NC). The first-order (h^{-1}) reactivation rate constant (k_r) was determined by transforming the percentage of AChE activity into the percentage of AChE inhibition where the slope of the linear regression of the natural log (ln) of the terminal portion of the curve equals the k_r (Levine and Murphy, 1977).

Pharmacodynamic model development. Pharmacodynamic models describing the *in vitro* interaction of the oxons with AChE were developed in SIMuSOLV® (Trademark of the Dow Chemical Co., Midland, MI), as described previously (Kardos and Sultatos, 2000). The first model, referred to as the active binding site model, used the inhibitory rate constant (k_i) based on the equation derived by Main (1964); the second model, referred to as the peripheral binding site model, included equations describing a secondary oxon binding site on the AChE molecule (Fig. 1). The differential equations that describe the active binding site model were as follows (Kardos and Sultatos, 2000):

$$\frac{d[AChE_{Phos}]}{dt} = k_i * [Oxon] * [AChE] - k_r * [AChE_{Phos}] \qquad (1)$$

$$[AChE] = [AChE_t] - [AChE_{Phos}] \qquad (2)$$

$$[Oxon] = [Oxon_t] - [Metab] \qquad (3)$$

where $\frac{d[AChE_{phos}]}{dt}$ represents the change in the amount of the phosphorylated AChE over time; $AChE_t$ represents total AChE active site concentration (nM); $AChE_{Phos}$ represents phosphorylated AChE concentration (nM); k_i is the apparent bimolecular inhibition rate constant of AChE ($nM^{-1}h^{-1}$); k_r is the apparent first-order reactivation rate constant of the phosphorylated enzyme (h^{-1}); $Oxon_t$ and $Oxon$ represent the starting total oxon concentration that was added to the incubation and the available oxon concentration within the incubation, respectively (nM); and *Metab* represents the major metabolites of CPO or PO (trichloropyridinol and *p*-nitrophenol, respectively).
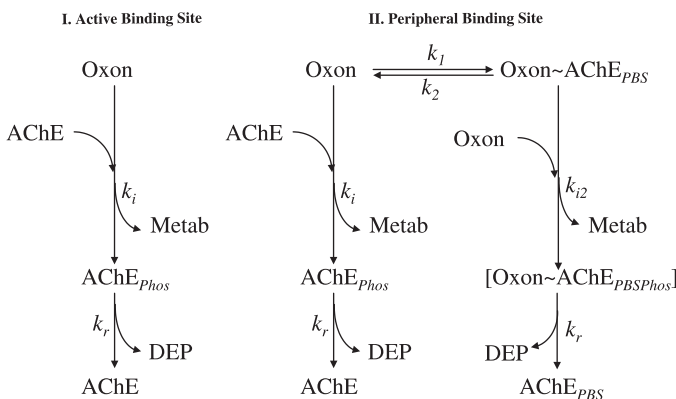

FIG. 1. Schematic diagram of the oxon interaction (CPO or PO) with the AChE active binding site (I) and with the active binding site that includes a putative peripheral binding site (II). The oxon molecule interaction with the active site, as described by the apparent bimolecular inhibition rate constant (k_i), resulted in an irreversibly inhibited AChE (AChE$_{Phos}$). Reversible binding of the oxon with the putative peripheral binding site of the AChE molecule (Oxon∼AChE$_{PBS}$) is described by a second-order binding rate constant (k_1) and first-order dissociation rate constant (k_2), leading to an altered apparent bimolecular inhibition rate constant (k_{i2}) and resulting in irreversible phosphorylation of AChE (Oxon∼$AChE_{PBSPhs}$). The "∼" symbol represents the reversible binding of the oxon to the peripheral binding site. In both cases, Metab represents the major metabolites of CPO or PO (trichloropyridinol and -*p*-nitrophenol, respectively); DEP is the diethylphosphate moiety; k_r is the apparent first-order reactivation rate constant of the phosphorylated enzyme; and AChE$_{PBS}$ is the recovered AChE molecule considering the putative peripheral binding site.

The differential equations describing the peripheral binding site model were as follows (Kardos and Sultatos, 2000):

$$\frac{d[AChE_{Phos}]}{dt} = k_i * [Oxon] * [AChE] - k_r * [AChE_{Phos}] \quad (4)$$

$$\frac{dOxon \sim AChE_{PBS}}{dt} = k_1 * [Oxon] * [AChE_{PBS}] - k_2 * [Oxon \sim AChE_{PBS}]$$
$$- k_{i2} * [Oxon] * [Oxon \sim AChE_{PBS}] \quad (5)$$

$$\frac{dOxon \sim AChE_{PBSPhos}}{dt} = k_{i2} * [Oxon] * [Oxon \sim AChE_{PBS}]$$
$$- k_r * [Oxon \sim AChE_{PBSPhos}] \quad (6)$$

$$[AChE] = [AChE_t] - \{[Oxon \sim AChE_{PBS}] - [Oxon \sim AChE_{PBSPhos}]$$
$$- [AChE_{Phos}]\} \quad (7)$$

$$[Oxon] = [Oxon_t] - [Oxon \sim AChE_{PBS}] - [Metab] \quad (8)$$

where $\frac{dOxon \sim AChE_{PBS}}{dt}$ represents the change in the amount of the peripheral binding site occupied by oxon over time; k_1 is the second-order reversible binding rate constant of the oxon to the peripheral binding site ($nM^{-1}h^{-1}$); k_2 is the first-order dissociation rate constant (h^{-1}); k_{i2} is an altered apparent bimolecular inhibition rate constant ($nM^{-1}h^{-1}$) due to occupation of the binding site; and $\frac{dOxon \sim AChE_{PBSPhos}}{dt}$ is the change in the amount of the irreversibly phosphorylated AChE over time, considering the presence of peripheral binding site occupation. $AChE_t$ and $AChE$ represent the total $AChE$ concentration within the incubation and the available $AChE$ concentration within the incubation, respectively (nM). The "$\sim$" symbol represents the reversible binding of the oxon to the peripheral binding site. All other symbols are defined in Figure 1 or the active binding site model equations.

To solve the active binding site model equations (Equations 1–3), the initial AChE active site concentration and k_r values had to be determined experimentally. Titration of brain AChE enzyme with known oxon concentrations (5×10^{-4}–0.01 nM) was used to estimate the total concentration of active sites while k_r was determined as described above (Kardos and Sultatos, 2000; Kousba *et al.*, 2003; Levine and Murphy, 1977). The initial AChE active site estimation was calculated based on the enzyme inhibition obtained for a given oxon concentration. The model optimization was used to estimate the final rat brain AChE active site concentration and the bimolecular inhibition rate constant (k_i; $nM^{-1}h^{-1}$) of CPO and PO toward rat brain AChE as a function of varying oxon concentrations (5×10^{-4}–100 nM). The k_i was also estimated using the method of Main (1964) at higher CPO and PO concentrations (1–100 nM), selected to give a maximum inhibition ranging from 10–90% over a 5- to 30-min incubation period. The log percentage of activity was plotted against time and the slopes of each log plot were calculated using linear regression. These slopes were used for the final k_i calculation.

To solve the peripheral binding site model equations (Equations 4–8), the initial values for the model parameters (k_i, k_{i2}, k_r, and total enzyme concentration) were based on the active binding site model optimization. Estimates of k_1 and k_2 and the final parameter values for k_i, k_{i2}, k_r, and total enzyme concentration were determined by optimization of the peripheral binding site model against several experimental data sets. The peripheral binding site model was only applied to fit the whole data sets for AChE inhibition by PO due to the robust amount of data that were generated. Also, comparison of the k_i estimated values for the more limited data of AChE inhibition by CPO at different concentrations was consistent with the same relationship observed following incubation with PO.

RESULTS

A comparison of the *in vitro* AChE dynamic response in brain homogenates incubated with 1 pM CPO and PO is shown in
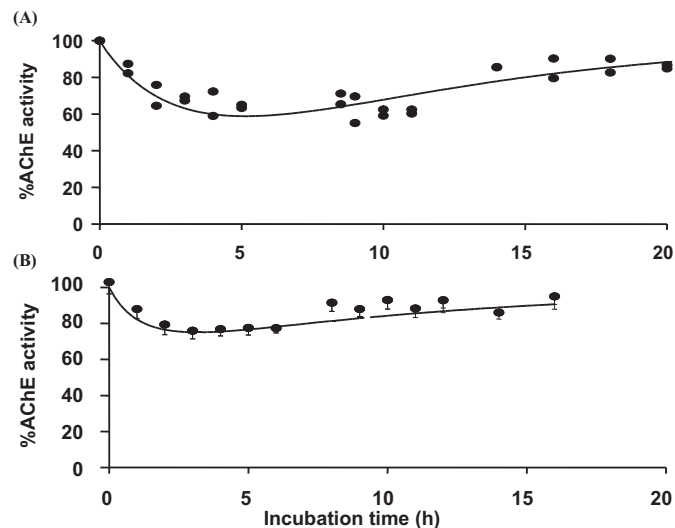

FIG. 2. *In vitro* pharmacodynamic model simulation of AChE inhibition against experimental data determined by the rate of ATC hydrolysis. The data are expressed as percentages of total AChE activity and represent either the individual data points for samples incubated with (A) 1×10^{-3} nM PO or (B) mean $\pm$ SD of three determinations for samples incubated with CPO. The lines represent model optimizations against AChE inhibition. The model was optimized for k_i and enzyme active site concentration while using the experimentally determined k_r values (see Fig. 3). The k_i estimates for AChE inhibition by CPO and PO were 150–180 (two determinations) and 300 ± 180 $nM^{-1}h^{-1}$, respectively.

Figure 2. At this low oxon concentration, the total brain AChE activity was inhibited $\sim$30 and 40% by 3–4 h following incubation with CPO and PO, respectively. An initial estimate of total AChE within the incubation mixture was $\sim$2 pM; however, an exact calculation was difficult since both reactivation and inhibition of AChE occur simultaneously and due to the difficulty in experimental determination of an exact point of maximal AChE inhibition. The dynamic model made it possible to determine a more accurate estimation for AChE concentration by maintaining the k_r at the experimentally determined values while optimizing to fit the data for the k_i and active site concentration. The active binding site model optimization at 1×10^{-3} nM oxon concentrations resulted in an estimated enzyme active site concentration of 0.002 ± 0.0007 nM/incubation and k_i values of 150–180 (two determinations) and 300 ± 180 $nM^{-1}h^{-1}$ for CPO and PO, respectively. The k_r for AChE were 0.084–0.087 (two determinations) and 0.091 ± 0.023 h^{-1} for CPO and PO, respectively (Fig. 3). Based on the brain dilution used in the current assay, the enzyme concentration represented an actual AChE content of 0.09 ± 0.03 nmole/brain, which is consistent with the value of the 0.11 nmole/brain reported by Maxwell *et al.* (1987).

While the estimated k_i values reasonably described AChE response following incubation with 1×10^{-3} nM oxon, those same k_i values markedly overestimated brain AChE inhibition at higher oxon concentrations, as shown in Figure 4. Model optimization against the higher concentrations resulted in k_i estimates of 0.0412 $nM^{-1}h^{-1}$ for AChE inhibition by PO.
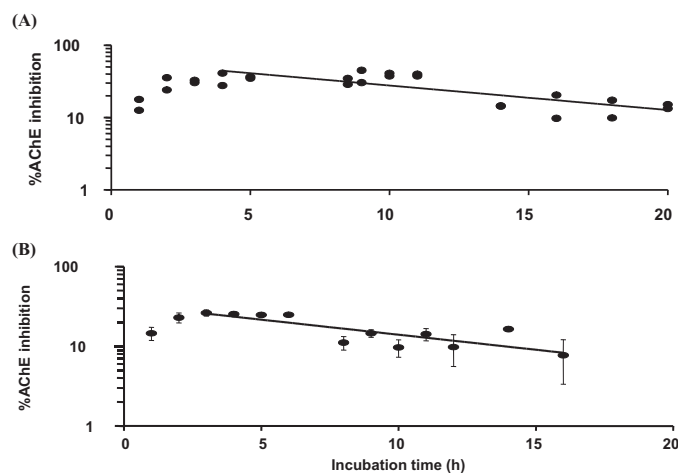
FIG. 3. *In vitro* determination of rat brain AChE spontaneous reactivation rate constant (k_r) following inhibition by (A) 1×10^{-3} nM PO and (B) CPO. The data are expressed as percentages of total AChE inhibition and represent either the individual data points for samples incubated with 1×10^{-3} nM PO or mean $\pm$ SD of three determinations for samples incubated with CPO. The lines represent the best fit for the terminal portion of the curve using linear regression where the corresponding k_r value equals the slope of the line. The spontaneous reactivation rates of the inhibited AChE for CPO and PO were 0.084–0.087 (two determinations) and 0.091 ± 0.023 h^{-1}, respectively.
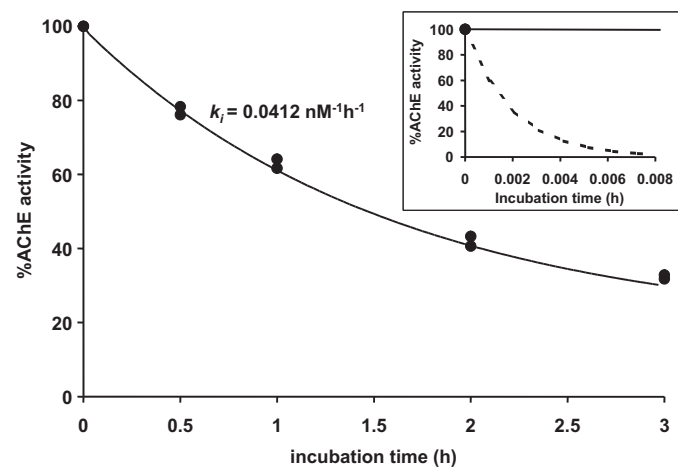

FIG. 4. Comparison of the experimental data and active binding site model output with a best-fit k_i, for an AChE concentration of 1.51×10^{-3} nM and a PO concentration of 2 nM. The data (individual points) are expressed as percentages of total AChE activity and the solid line represents the model simulation using the best-fit k_i. The inset shows the model output (dashed line) using the k_i determined in Figure 2A and suggests marked overestimation of the rate and degree of AChE inhibition.

Hence, the k_i values describing AChE inhibition by high oxon concentrations were much lower relative to those describing the AChE inhibition by 1×10^{-3} nM oxon.

The relationship between the resultant k_i and the oxon concentrations is shown in Figure 5. This analysis shows that, at low PO concentrations (5×10^{-4} to <1 nM), the k_i ranges from 420 to ~0.30 nM^{-1}h^{-1} and demonstrates a relatively linear change as
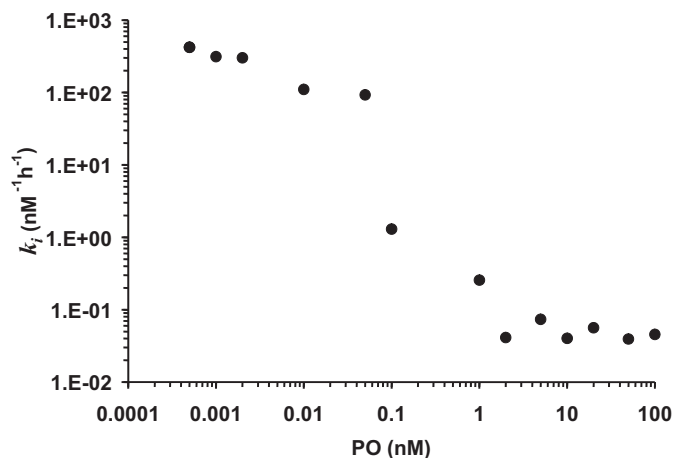

FIG. 5. The relationship between k_i values and PO concentrations (5×10^{-4}–100 nM) where the k_i values were determined using the model optimizations. The k_i at 5×10^{-4} nM PO concentration was 420 nM^{-1}h^{-1} and the k_{i2} at an infinitely high oxon concentration (plateau) was 0.0216 nM^{-1} h^{-1}.

a function of PO concentration. Higher PO concentrations (1–100 nM) resulted in a substantially lower k_i (0.250 to 0.019 nM^{-1}h^{-1}) and were relatively insensitive to changes in oxon concentration. Similar relationships between k_i values and oxon concentrations were reported for mouse brain AChE and recombinant AChE inhibition by PO and methyl-PO (Kardos and Sultatos, 2000).

Estimates of k_i for CPO and PO towards AChE were also determined experimentally using the method of Main (1964) and the results are shown in Figures 6 and 7. Based on this analysis, the k_i for CPO and PO towards AChE were estimated to be 0.206 ± 0.018 and 0.0216 nM^{-1}h^{-1}, respectively. To further substantiate these estimates, the k_i was also determined using the active binding site model optimization by varying the k_i value while maintaining the parameter estimates for the total enzyme active site concentration and the k_r at experimentally determined values. The model was simultaneously fit to all experimental data sets and the results are shown in Figure 8. Based on this model optimization, k_i values of 0.380 ± 0.032 and 0.0444 nM^{-1}h^{-1} resulted in a best fit to the data and were reasonably consistent (i.e., factor of 2) with the 0.206 ± 0.018 and 0.0216 nM^{-1}h^{-1} determined by linear regression analysis for CPO and PO, respectively. These results for CPO and PO were also reasonably consistent with previously reported estimates determined at nM oxon concentrations (Amitai *et al.*, 1998; Carr and Chambers, 1996; Kardos and Sultatos, 2000; Rosenfeld *et al.*, 2001). However, it should be noted that no reported data were found for k_i estimates following AChE inhibition that use low oxon concentrations (pM) similar to those used in this study.

The peripheral binding site model developed for PO in this study was intended to describe the *in vitro* AChE inhibition over a wide range of oxon concentrations. In this model, the k_i had two possible theoretical values depending on whether or not the
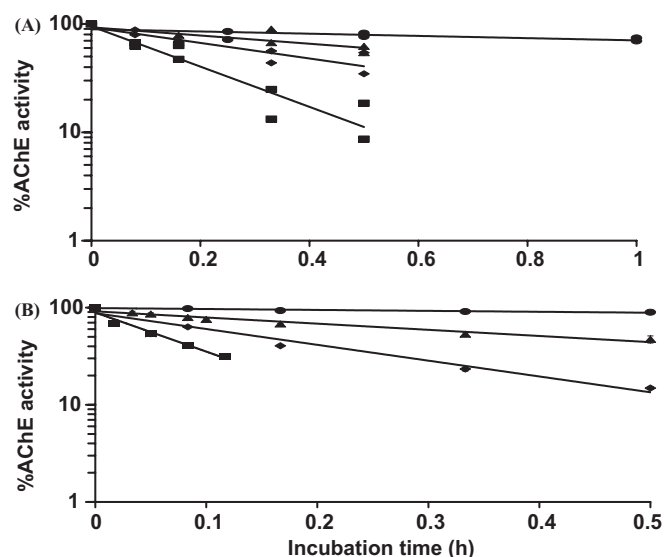
FIG. 6. *In vitro* rat brain AChE activity as determined from the rate of ATC substrate hydrolysis (mOD/min) as a function of (A) PO and (B) CPO concentrations for different incubation periods. The data are expressed as percentages of total AChE activity and represent either the individual data points for samples incubated with PO or mean ± SD of three determinations for samples incubated with CPO. (A) Circles, PO concentration of 10 nM; triangles, 20 nM; diamonds, 50 nM; and rectangles, 100 nM. (B) Circles, CPO concentration of 1 nM; triangles, 5 nM; diamonds, 10 nM; and rectangles, 25 nM. The lines represent the best fit from linear regression analysis for each data set and the slopes obtained from regression analysis showed a correlation >0.95 and were used for the final k_i calculation, as shown in Figure 7.
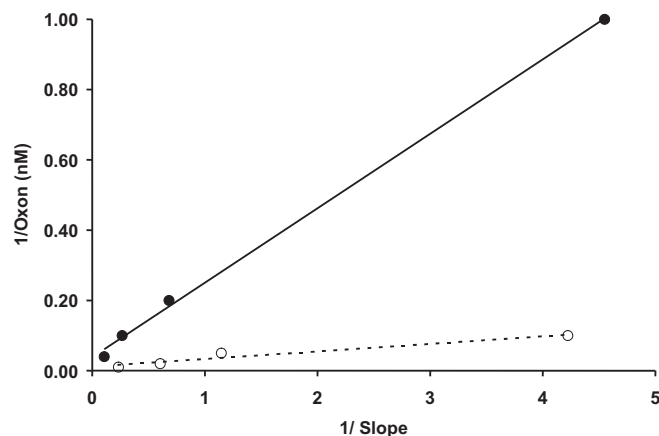

FIG. 8. K_i calculation using the k_i pharmacodynamic model optimizations against the experimental data. The data are expressed as percentages of total AChE activity and represent either the individual data points for samples incubated with PO or mean ± SD of three determinations for samples incubated with CPO. (A) Circles, PO concentration of 10 nM; triangles, 20 nM; diamonds, 50 nM; and rectangles, 100 nM. (B) Circles, CPO concentration of 1 nM; triangles, 5 nM; diamonds, 10 nM; and rectangles, 25 nM. Each line represents the model simulation for a particular data set. The estimated k_i values were 0.380 ± 0.032 and 0.0444 nM^{-1}h^{-1} for CPO and PO, respectively.

FIG. 7. K_i determination plot. Each symbol represents a specific slope obtained from each data set (see Fig. 6) at a given concentration of PO (open circles) and CPO (filled circles). The straight lines represent the best fit from regression analysis and their slopes equal the k_i of PO (dashed line) and CPO (solid line) towards rat brain AChE, as determined using the Main (1964) approach. The k_i values for AChE inhibition were 0.206 ± 0.018 and 0.0216 nM^{-1}h^{-1} for CPO and PO, respectively.

peripheral binding site was occupied by the oxon. The peripheral binding site model assumed that one oxon molecule would irreversibly phosphorylate the serine hydroxyl group at the AChE active site but at a lower potency due to the effect induced by
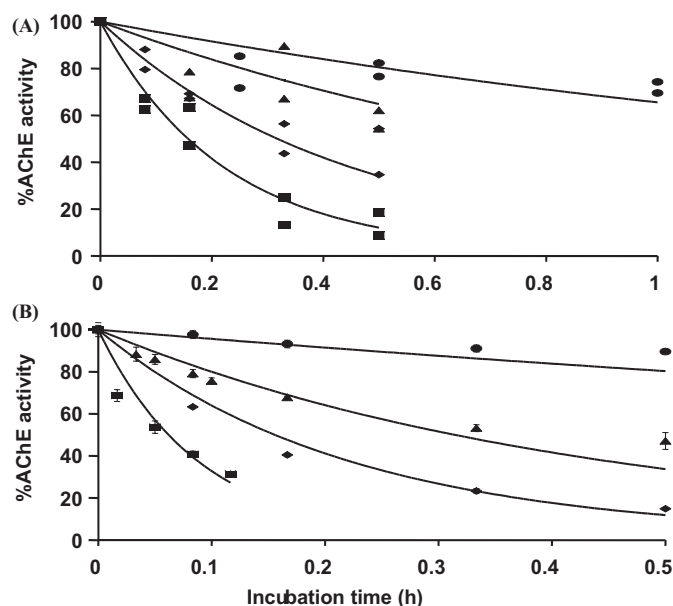
reversible binding of the peripheral binding site (Fig. 1 and Equations 4–6). Initial k_i estimates included theoretical maximal and minimal k_i values determined at low and high PO concentrations, where the peripheral binding site was theoretically assumed to be fully occupied or unoccupied by oxon. The association (k_1) and dissociation (k_2) rate constants for the reversible binding of the PO to the peripheral binding site (Fig. 1) were then estimated by model optimization against several AChE response data sets simultaneously; for the purpose of simplification, the k_r value was held constant. The results of the peripheral binding site model optimization revealed a single best solution for the AChE concentration, k_i and k_{i2}, but multiple solutions for k_1 and k_2. The value for k_1 that gave the best description for all of the generated AChE inhibition data sets indicated that the k_1 could have several values, as long as the k_1 was equal to or more than 10 while maintaining the ratio of k_1/k_2 at three (the association with the peripheral binding site was three time higher than the dissociation).

The final parameter estimates were used in the peripheral binding site model and the model was optimized simultaneously against AChE inhibition at several PO concentrations. The peripheral binding site model projected slight changes in the initial estimate of AChE active site concentration (0.0014 vs. 0.0015 nM determined by the active binding site model) and k_i (1450 vs.
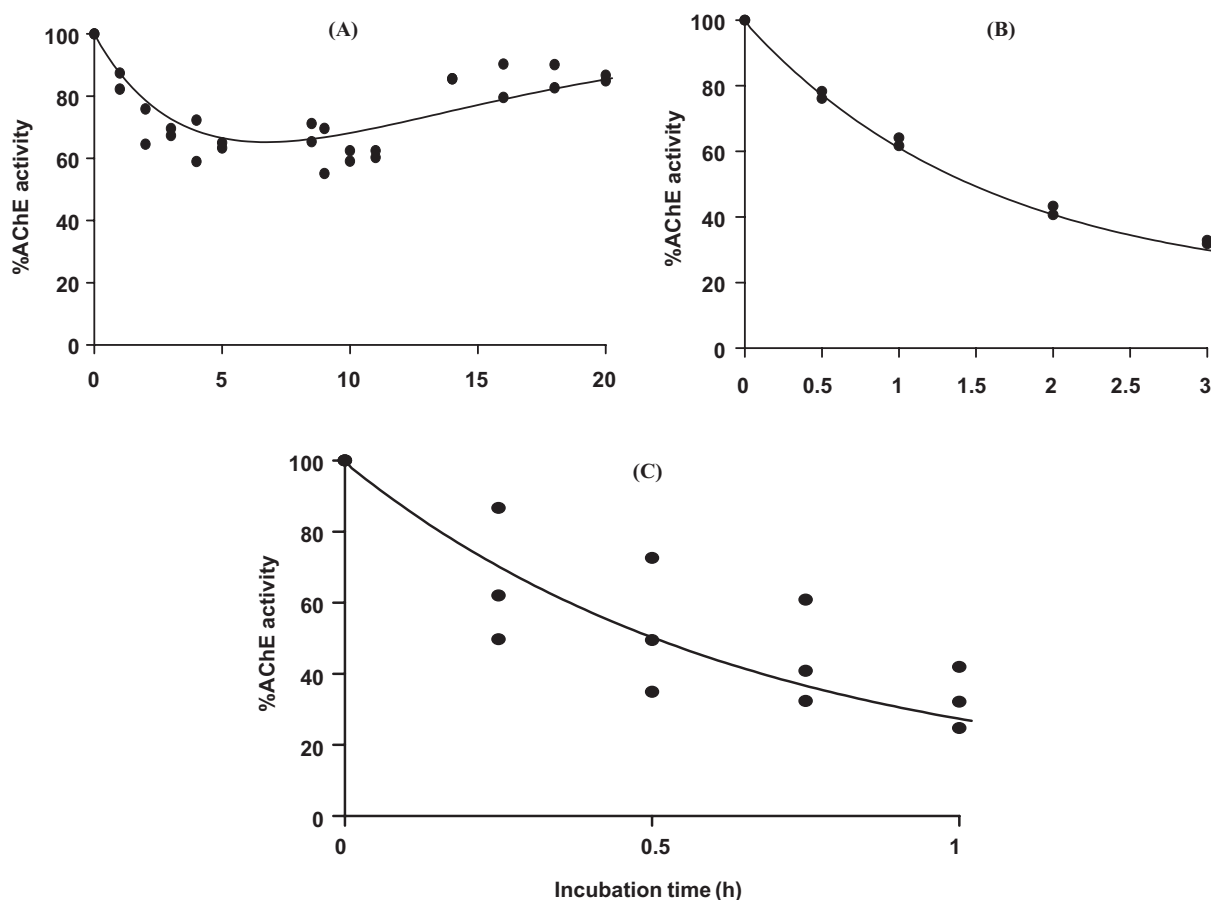
FIG. 9. Inhibition of rat brain homogenate AChE expressed as percentages of control with time at different PO concentrations. The data are presented as percentages of control activity versus the time at PO concentration of (A) 1×10^{-3} nM, (B) 2 nM, and (C) 10 nM. In all figures, the circles represent the experimental data while the solid lines represent the peripheral binding site model output simulations.

420 nM^{-1}h^{-1} determined by the active binding site model), which may be attributed to the fact that the active binding site model did not account for the oxon molecules bound to the peripheral binding site. Figure 9 shows the peripheral binding site model simulations against AChE inhibition at 1×10^{-3}, 2, and 10 nM PO. Figure 9 indicates that the inclusion of a peripheral binding site for the AChE molecule resulted in an adequate description of the enzyme inhibition and that the existence of such a site exerted a significant role in modulating the dynamic behavior of AChE.

DISCUSSION

Pharmacodynamic models seek to quantify biological responses as a result of chemical interactions with their target sites (Mager and Jusko, 2001; Maxwell *et al*., 1988). Biologically based modeling represents an effective tool for prediction of unexplainable biological events as evidenced by the use of the peripheral binding site model for predicting dynamics of AChE inhibition. The current study was conducted

to better characterize and compare the *in vitro* dynamics of AChE inhibition over a broad range of CPO and PO concentrations to evaluate the potential contribution of a peripheral binding site associated with AChE inhibition.

Prior to Kardos and Sultatos (2000), k_i determination studies were based on the method of Main (1964), assuming that the *in vitro* interaction between cholinesterase and OP approximated first-order conditions with respect to uninhibited enzyme concentration. Main (1964) used organophosphate concentrations much higher than the tissue homogenate cholinesterase (ChE) concentration, yielding a single k_i estimate of enzyme inhibition. The approach we used was a pharmacodynamic model describing the *in vitro* inhibition kinetics of AChE by CPO and PO (Kardos and Sultatos, 2000; Kousba *et al*., 2003). The pharmacodynamic model was coded to estimate the k_i under both first- and second-order conditions through model optimizations against experimental data. This method was proposed as a more robust technique for k_i estimation (Kardos and Sultatos, 2000; Kousba *et al*., 2003) and the results indicated a substantial difference in the k_i values compared with previous

studies (Amitai *et al.*, 1998; Carr and Chambers, 1996; Rosenfeld *et al.*, 2001). Although AChE inhibition, using high oxon concentrations, was markedly different, spontaneous reactivation of the inhibited enzyme was similar (Fig. 3). This is not surprising since the enzyme-inhibited form of AChE is similar in both situations and spontaneous reactivation mainly occurs due to hydrolysis of the phosphorylated bond. The k_r value of 0.091 ± 0.023 h^{-1} determined for AChE inhibited by PO is similar to the 0.070 h^{-1} reported by Kardos and Sultatos (2000) for mouse brain AChE, but slightly higher than 0.024 h^{-1} reported by Levine and Murphy (1977) in rats. The k_r values of 0.084–0.087 h^{-1} determined for AChE inhibited by CPO are higher than those reported by Carr and Chambers (1996), who estimated similar k_r values (0.0140 and 0.0148 h^{-1}) for AChE inhibited by CPO and PO at 37°C. Pope *et al.* (1991) reported that, among different OP insecticides, cholinesterase recovery *in vivo* is probably related to differences in absorption, biotransformation, and, most importantly, spontaneous enzyme reactivation. The k_i values describing AChE inhibition following incubation with 1 pM oxon were >1000 and 10,000 times higher than those values determined using the nM range concentrations for CPO and PO, respectively (compare Figs. 2 and 7). However, the k_i values determined for both CPO and PO at higher oxon concentrations (1–100 nM; Figs. 5, 7, and 8) were approximately similar to previously reported values. These results suggest that the pharmacodynamic modeling is a sound approach for k_i estimation over a broad range of oxon concentrations.

As shown in Figure 2, the active binding site model optimization reasonably described AChE inhibition at a 1×10^{-3} nM oxon concentration; however, using those k_i values resulted in an overestimation of AChE inhibition at higher oxon concentrations. The estimated k_i values that described AChE inhibition at 1×10^{-3} nM oxon concentrations were more than three orders of magnitude greater that the estimated k_i at nM concentrations. In essence, the high oxon concentrations resulted in a lower k_i value, which reflects a lower capacity to phosphorylate the serine OH group of the active site of AChE. At lower oxon concentrations, the phosphorylation of AChE was more efficient (compare Figs. 2 and 7). Likewise, Kardos and Sultatos (2000) estimated a 10-fold higher k_i value for brain AChE incubation with 0.1 nM PO compared with the k_i value following 100 nM.

As described by Kardos and Sultatos (2000), several explanations for the oxon concentration–dependent k_i values have been considered, including the existence of multiple forms of AChE and excess substrate inhibition of AChE. Whereas several isoforms of AChE have been identified, all are products of one gene; their catalytic cores are identical, exhibiting similar susceptibility to inhibition, and only differ in their mechanism of anchoring (Friboulet *et al.*, 1990; Sussman *et al.*, 1991). This implies that isoforms of AChE are unlikely to differ in their response to inhibition by different organophosphate concentrations by more than four orders of magnitude, as shown in Figures 1 and 5. A more plausible explanation, consistent with the results obtained in this study, is based on AChE being inhibited by its own substrate, acetylcholine, as a result of allosteric modification or blockage of the active site. Allosteric modification or blockage are due to acetylcholine binding to a peripheral site and preventing access of other substrate molecules to the active site (Taylor and Radic, 1994). The occupation of the proposed secondary binding site may prevent the substrates from reaching the active site of the AChE molecule, resulting in slower rates of phosphorylation of AChE at high oxon concentrations (Fig. 1).

Rat brain AChE activity following incubation with a high oxon concentration showed more *in vitro* inhibition by CPO than PO, as evidenced by the lower IC$_{50}$ and higher k_i values for CPO compared with those of PO. The estimated *in vitro* IC$_{50}$ for CPO was ∼10 times lower than for PO (8.98 vs. 81.66 nM, respectively), which is consistent with previously reported relationships (Atteberry *et al.*, 1997; Mortensen *et al.*, 1998). The k_i values determined for CPO and PO inhibition of AChE in this study were also consistent with Amitai *et al.* (1998), who estimated a CPO k_i of 9–11 times greater than for PO. The basis of this inhibitory potency difference is not fully understood since the enzyme inhibition complex for the two substrates are chemically identical (Table 1). Carr and Chambers (1996) suggested that the potency difference may be attributed to the differences in the interaction of the leaving group with the active site, whereby the association of the leaving group moiety with the anionic site may produce an environment that affects the rate of phosphorylation of the active site by inducing conformational changes in the tertiary structure of the enzyme. In contrast to the observed *in vitro* potency for AChE inhibition, parathion was appreciably (>30 times) more acutely toxic than chlorpyrifos (LD$_{50}$ values of 4–13 and 82–155 mg/kg, respectively; Gaines, 1969). This *in vivo* potency difference is primarily a reflection of the higher capacity for metabolic detoxification of chlorpyrifos compared to parathion (Atteberry *et al.*, 1997; Chambers *et al.*, 1990; Chanda *et al.*, 1998).

Of particular interest in our study was the observation that, at low oxon concentrations, comparable k_i values for CPO and PO were obtained versus a 10- to 15-fold difference following incubation at a nM oxon concentration range (Figs. 2 and 7). The lowest oxon concentration (1 pM) used in this study was two orders of magnitude lower than what Kardos and Sultatos (2000) used and has facilitated the comparison of the inhibitory potency of CPO and PO at disparate (high vs. low) oxon concentrations with respect to the potential secondary binding site occupation by the oxons. Following incubation with high oxon concentrations, all peripheral binding sites were assumed to be fully occupied; at low concentrations, the peripheral binding sites were assumed to be minimally occupied, as evidenced by partial AChE inhibition. A possible explanation for this phenomenon is that the difference in AChE phosphorylation could be attributed to a difference in the occupancy of the peripheral binding site (excess substrate inhibition site). At low oxon concentration, both oxons have similar accessibility to the enzyme active site yielding similar k_i. Since CPO and

PO share a common diethyl phosphate metabolite that is responsible for binding and inactivation of AChE, it is reasonable to assume that they would exhibit similar inhibition kinetics for AChE. Therefore, the similarity in inhibitory capacity at low oxon concentration is biologically plausible based on the stochiometric interaction of OP with cholinesterase, suggesting that other chemically related phosphorothioate insecticides would behave similarly following *in vitro* interaction with AChE. Nevertheless, additional *in vitro* studies are needed for validation.

The results of this study suggest the presence of a peripheral binding site that may play an important role in determining the biological interaction of AChE with CPO and PO and potentially other OP insecticides. This may be of particular relevance in understanding the dynamics associated with exposures at low, environmentally relevant levels. Our data clearly characterized the different k_i values for the inhibition of rat brain AChE by PO and CPO under various *in vitro* kinetic scenarios and indicated that the estimated k_i values are significantly affected by the oxon concentrations, which may be explained by the presence of a proposed secondary binding site on AChE. Still, more studies are needed to further assess the cholinesterase response to other insecticides in different species. Also, it should be noted that changing the phosphorylation capacity of the oxon molecules following *in vitro* incubation of AChE with different oxon concentrations has not been confirmed with the *in vivo* exposure studies; therefore, the possibility of an *in vivo* concentration effect needs more investigation.

ACKNOWLEDGMENTS

REFERENCES

Amitai, G., Moorad, D., Adani, R., and Doctor, P. (1998). Inhibition of acetylcholinesterase and butyrylcholinesterase by chlorpyriphos-oxon. *Biochem. Pharmacol.* **56,** 293–299.

Atteberry, T., Burnett, T., and Chambers, J. (1997). Age-related differences in parathion and chlorpyrifos toxicity in male rats: Target and nontarget esterase sensitivity and cytochrome P450–mediated metabolism. *Toxicol. Appl. Pharmacol.* **147,** 411–418.

Berman, H. A., and Leonard, K. (1992). Interaction of tetrahydroaminacridine with acetylcholinesterase and butyrylcholinesterase. *Mol. Pharmacol.* **41,** 412–418.

Berman, H. A., Yguerabide, J., and Taylor, P. (1980). Fluorescence energy transfer on acetylcholinesterase: Spatial relationship between peripheral and active centers. *Biochemistry* **19,** 2226–2235.

Carr, L. R., and Chambers, J. E. (1996). Kinetic analysis of *in vitro* inhibition, aging, and reactivation of brain acetylcholinesterase from rat and channel cat fish by paraoxon and chloropyrifos-oxon. *Toxicol. Appl. Pharmacol.* **139,** 365–373.

Chambers, H. W., Brown, B., and Chambers, J. E. (1990). Noncatalytic detoxification of six organophosphorus compounds by rat liver homogenates. *Pesti. Biochem. Physiol.* **36,** 308–315.

Chanda, S. M., Mortensen, S. R., Moser, V. C., and Padilla, S. (1998). Tissue-specific effects of chlorpyriphos on carboxylesterase and cholinesterase activity in adult rats: An *in vitro* and *in vivo* comparison. *Fundam. Appl. Toxicol.* **38,** 3807–3811.

Changeux, J. P. (1966). Responses of acetylcholinesterase from Torepo Marmorata to salts and curarizing drugs. *Mol. Pharmacol.* **2,** 369–392.

Ellman, G., Courtney, D., and Andres, V. (1961). A new and rapid colorimetric determination of acetylcholinesterase activity. *Biochem. Pharmacol.* **7,** 88–95.

Friboulet, A., Rieger, F., Goudou, D., Amitai, G., and Taylor, P. (1990). Interaction of an organophosphate with a peripheral site on acetylcholinesterase. *Biochemistry* **29,** 914–920.

Gaines, T. B. (1969). Acute toxicity of pesticides. *Toxicol. Appl. Pharmacol.* **14,** 515–534.

Kardos, S. A., and Sultatos, L. G. (2000). Interactions of the organophosphate paraoxon and methyl paraoxon with mouse brain acetylcholinesterase. *Toxicol. Sci.* **58,** 118–126.

Kousba, A., Poet, T. S., and Timchalk, C. (2003). Characterization of the *in vitro* kinetic interaction of chlorpyrifos-oxon with rat salivary cholinesterase: A potential biomonitoring matrix. *Toxicology* **188**(2–3), 219–232.

Levine, B., and Murphy, S. (1977). Esterase inhibition and reactivation in relation to piperonyl butoxide– phosphorothionate interactions. *Toxicol. Appl. Pharmacol.* **40,** 379–391.

Mager, D. E., and Jusko, W. J. (2001). Pharmacodynamic modeling of time-dependent transduction systems. *Clin. Pharmacol. Ther.* **70,** 210–216.

Main, A. R. (1964). Affinity and phosphorylation constants for the inhibition of esterases by organophosphates. *Science* **144,** 992–993.

Maxwell, D. M., Lenz, D. E., Groff, W. A., Kaminkis, A., and Forehlich, H. L. (1987). The effects of blood flow and detoxification on *in vivo* cholinesterase inhibition by soman in rats. *Toxicol. Appl. Pharmacol.* **88,** 66–76.

Maxwell, D. M., Vlabacos, C. P., and Levy, D. E. (1988). A pharmacodynamic model for soman in the rat. *Toxicol. Lett.* **43,** 175–188.

McCracken, N. W., Blain, P. G., and Williams, F. M. (1993). Nature and role of xenobiotic metabolizing esterases in rat liver, lung, skin and blood. *Biochem. Pharmacol.* **45**(1), 31–36.

Mileson, B. E., Chambers, J. E., Chen, W. L., Dettbarn, W., Ehrich, M., Eldefrawi, A. T., Gaylor, D. W., Hamernik, K., Hodgson, E., Karczmar, A. G., *et al.* (1998). Common mechanism of toxicity: A case study of organophosphorus pesticides. *Toxicol. Sci.* **41,** 8–20.

Mortensen, S. R., Brimijoin, S., Hooper, M. J., and Padilla, S. (1998). Comparison of the *in vitro* sensitivity of rat acetylcholinesterase to chlorpyrifos-oxon: What do tissue IC$_{50}$ values represent? *Toxicol. Appl. Pharmacol.* **148,** 46–49.

Mortensen, S. R., Chanda, S. M., Hooper, M. J., and Padilla, S. (1996). Maturational differences in chlorpyrifos-oxonase activity may contribute to age-related sensitivity to chlorpyrifos. *J. Biochem. Toxicol.* **11,** 279–287.

Nostrandt, A. C., Duncan, J. A., and Padilla, S. (1993). A modified spectrophotometric method appropriate for measuring cholinesterase activity in tissue from carbamate-treated animals. *Fundam. Appl. Toxicol.* **21,** 196–203.

Poet, T. S., Wu, H., Kousba, A., and Timchalk, C. (2003). *In vitro* rat hepatic and enterocyte metabolism of the organophosphate pesticides chlorpyrifos and diazinon. *Toxicol. Sci.* **72,** 193–200.

Pope, C. N., Chakraborti, T. K., Champan, M. L., Farrar, J. D., and Arthun, D. (1991). Comparison of *in vivo* cholinesterase inhibition in neonatal and adult rats by three organophosphothioate insecticides. *Toxicology* **68,** 51–61.

Rosenfeld, C., Kousba, A., and Sultatos, L. G. (2001). Interactions of rat brain acetylcholinesterase with the detergent Triton X-100 and the organophosphate paraoxon. *Toxicol. Sci.* **63,** 208–213.

Sultatos, L. G., and Murphy, S. D. (1983). Kinetic analyses of the microsomal biotranformation of the phosphorothioate insecticides chlorpyrifos and parathion. *Fundam. Appl. Toxicol.* **3,** 16–21.

Sussman, J. L., Harel, M., Frolow, F., Oefner, C., Goldman, A., Toker, L., and Silman, I. (1991). Atomic structure of acetylcholinesterase from torpedo Californiaca: A prototype acetylcholine-binding protein. *Science* **235,** 872–879.

Taylor, P., and Lappi, S. (1975). Interaction of fluorescence probes with acetyl-cholinesterase: The site and specificity of propidium binding. *Biochemistry* **14,** 1989–1997.

Taylor, P., and Radic, Z. (1994). The cholinesterases: From genes to proteins. *Annual Rev. Pharmacol. Toxicol.* **34,** 281–320.

Timchalk, C. (2001). Organophosphate pharmacokinetics. In *Handbook of Pesticide Toxicology* (R. Krieger, J. Doull, D. Ecobichon, D. Gammon, E. Hodgson, L. Reiter, and J. Ross, Eds.), Vol. 2, pp. 929–951. Academic Press, San Diego.

Timchalk, C., Nolan, R. J., Mendrala, A. L., Dittenber, D. A., Brzak, K. A., and Mattsson, J. L. (2002). A physiologically based pharmacokinetic and pharmacodynamic (PBPK/pharmacodynamic) model for the organo phosphate insecticide chlorpyrifos in rats and humans. *Toxicol. Sci.* **66,** 34–53.